Supporting Information

Constructing carbon nanotube-optimized hollow Ti_3C_2 MXene hierarchical conductive networks for robust lithium-sulfur batteries

*Ran Liu, Shengjun Zhai, Zimujun Ye, Mengzhu Liu, Yang Xu, Changwen Li, Xianbao Wang and Tao Mei**

Hubei Collaborative Innovation Center for Advanced Organic Chemical Materials, Overseas Expertise Introduction Center for Discipline Innovation (D18025), Key Laboratory for the Green Preparation and Application of Functional Materials, Hubei Key Laboratory of Polymer Materials, School of Materials Science and Engineering, Hubei University, Wuhan 430062, PR China

*Email Address: meitao@hubu.edu.cn; Fax: +86 27 8866 1729; Tel: +86 27 8866 2132

Contents

Figure S6 CV curves of the S/Ti_3C_2 HS electrode at scan rates of 0.1-0.5 mV s^{-1}.

Figure S7 Linear fits the peak current values of the cells with S/Ti_3C_2@N-CNTs and S/Ti_3C_2 HS based on the CV curves.

Figure S8 (a,b) Galvanostatic intermittent titration technique (GITT) curves of the different electrodes,(c) Migration coefficients of the Li^+.

Figure S9 Contact angles of (a) S/Ti_3C_2@ N-CNTs, (b) S/Ti_3C_2 HS by using electrolytes.

Figure S10 LSV curves of S/Ti_3C_2 HS and S/Ti_3C_2@ N-CNTs toward LiPSs oxidation, inset is the Tafel curve calculated from the peak A.

S2.2Tables:

Table S1. Summary of element contents in Ti_3C_2@N-CNTs determined by XPS.

Table S2. Nitrogen species of N 1s in Ti_3C_2@N-CNTs determined by XPS.

Table S3 Summary of recent reports on sulfur host cathodes for LSBs compared to Ti_3C_2@N-CNTs.

S1 Experimental Section

S1.1 Chemicals

Ti_3AlC_2 powder, polymethyl methacrylate(PMMA), lithium fluoride (LiF), hydrochloric acid(HCl), dicyandiamide, sulfur powder, acetylene black, polyvinylidene difluoride (PVDF), 1,2-dimethoxymethane (DME), 1,3-dioxolane (DOL), and 1-methyl-2-pyrrolidinone (NMP). All the above drugs can be purchased from the market without further purification.

S1.2 Material Synthesis

Synthesis of Ti_3C_2 MXene nanosheets

First, 1.6 g of LiF was slowly dissolved into 20 ml of 9.0 mol L^{-1} hydrochloric acid solution and stirred for 10 minutes. 1 g of Ti_3AlC_2 powder was gradually added to the above solution and stirred for 24 hours at 45 °C. The etched black solution was centrifuged, and washed with deionized water to pH ≥ 6 and the precipitate was then dissolved in 50 ml of deionized water. The dispersion was sonicated for 1 hour under argon and centrifuged at 3500 rpm for 30 minutes. The upper green suspension was used as several layers of Ti_3C_2 MXene dispersion and collected.

Synthesis of MXene/PMMA spheres

$Ti_3C_2T_X$ colloidal solution (2 mg mL^{-1}) was added dropwise to the PMMA sphere dispersion (10 mg mL^{-1}) under vigorous stirring and kept stirring for 30 minutes. The mass ratio of $Ti_3C_2T_X$ to PMMA spheres was controlled at 1:10. The mixture was then centrifuged at 3500 rpm for 20 minutes, and the solid residue was washed with distilled water and centrifuged again. Finally, the solid precipitate was collected and dried under vacuum at 60 °C to obtain $Ti_3C_2T_X$/PMMA hybrid spheres.

Synthesis of Ti_3C_2@N-CNTs hollow nanostructure

The prepared $Ti_3C_2T_X$/PMMA was ground and dispersed into a solution of $Co(NO_3)_3 \cdot 6H_2O$ at a concentration of 2.5 wt% and stirred for 2 hours. The product was then collected by centrifugation and washed at least once with distilled water. The solid

product was obtained by vacuum drying. The above impregnated Co product and dicyandiamide were then placed downstream and upstream of the tube furnace in a 1:6 mass ratio and annealed at 750 ℃ for 2 hours under a reducing atmosphere with a 9:1 composition of argon and hydrogen at a heating rate of 5 °C min^{-1}. The powder obtained was then immersed in a 1 mol L^{-1} HCl solution and shaken for 4 hours to remove the exposed cobalt nanoparticles. The resulting product is denoted as Ti_3C_2@N-CNTs.

Synthesis of Ti_3C_2 HS

The $Ti_3C_2T_X$/PMMA hybrid spheres were annealed at 750 °C under flowing argon for 2 hours to remove the PMMA and then cooled to room temperature to collect Ti_3C_2 hollow spheres.

Synthesis of S/Ti_3C_2@N-CNTs and S/Ti_3C_2 HS composites

The active material sulfur was successfully loaded into the host material by using the melt diffusion method. The S/Ti_3C_2@N-CNTs composites were obtained by mixing the sulfur and the synthesized Ti_3C_2@N-CNTs in a 7:3 mass ratio, sealing them in a reactor liner containing the argon atmosphere and then maintaining them at 155 °C for 12 hours. As a control, S/Ti_3C_2 HS composites were prepared similarly.

S1.3 Characterization

The morphologies and crystal structure were observed by field-emission scanning electron microscopy (FESEM) (ZEISS, Germany), transmission electron microscopy (TEM) (JEOL 2100F, Japan), and high-resolution TEM (HRTEM). Energy dispersive X-ray spectroscopy (EDS, JSM6510LV, Japan) was employed to represent the distribution of the measured elements. The crystal structure of the material was analyzed by X-ray diffraction (XRD) (D8-advance diffractometer, Bruker, Germany). The degree of graphitization of carbon materials was characterized using test light with a wavelength of 532 nm in a Raman spectrometer (Raman, Renishaw in Via). The nitrogen adsorption−desorption isothermal measured with an ASAP (2020 HD88, USA) analyzer can obtain the specific surface area and the pore size distribution information. The sulfur content was probed using the thermogravimetric analysis

technique (TGA) (Diamond TG-DTA, USA) under an N_2 atmosphere. X-ray photoelectron spectroscopy (XPS) (PHOIBOS 150, Germany) was used to analyze the chemical state of elements. UV-vis absorption spectrum was obtained on a UV-3600 Plus spectrometer (UV-3600 Plus, Shimadzu, Japan).

S1.4 Electrochemical measurements

The as-prepared cathode composites, acetylene black, and PVDF were mixed with a mass ratio of 7:2:1 and dispersed in NMP to prepare a homogeneous solvent and then it was bladed on the carbon-coated aluminum foil. Furthermore, it was necessary to undergo vacuum drying treatment to fully volatilize the solvent (NMP). Electrochemical tests were performed on CR 2016 coin cells, in which the anode was Li foil, the separator was a polyethylene membrane, and 1.0 mol L^{-1} bis-(trifluoromethane)sulfonimide lithium salt (LiTFSI) was dissolved in a DOL: DME (v/v = 1/1) mixed solvent with 2.0 wt% $LiNO_3$ to form the electrolyte. The typical sulfur loading per electrode was about 1.2-1.4 mg cm^{-2} and the electrolyte volume was 30 μL. Cyclic voltammetry (CV) was performed by scanning at 0.1 mV s^{-1} in the range of 1.7-2.8 V under an electrochemical workstation (CHI760E). Electrochemical impedance spectroscopy (EIS) spectra were also collected on it in the frequency range from 100,000 to 0.01 Hz.

Visualized adsorption tests

Li_2S_6 solutions (10 mmol L^{-1}) were prepared by dissolving S and Li_2S (the molar ratio is 5:1) in a mixture of DOL and DME (v/v = 1:1) and stirring vigorously at 60 °C for 12 h. To evaluate the adsorption performance of LiPSs, 20 mg of active materials (Ti_3C_2@N-CNTs and Ti_3C_2 HS) was added to 4 mL Li_2S_6 solution with 30 seconds of shaking and standing for a while. The supernatant was characterized by UV-vis and the precipitates were detected by XPS. All the above operations were carried out in an argon-filled glove box.

Li_2S nucleation and decomposition tests

For the study of liquid-solid conversion kinetics, Li_2S_8 solution (0.2 mol L^{-1}) was prepared by mixing S and Li_2S (molar ratio 7:1) and dissolving the mixture in DME and DOL (v/v = 1:1)solution containing 1.0 mol L^{-1} LiTFSI under vigorous stirring. Celgard 2400 membrane was used as the separator. The prepared Ti_3C_2@N-CNTs and Ti_3C_2 HS were used as cathodes and the lithium foil as anodes. 20 μL Li_2S_8 was dropped onto the cathode and 20 μL of conventional LiTFSI electrolyte was added to the anode side. During nucleation measurements, the fresh cells were galvanostatically discharged to 2.06 V at 0.112 mA. Subsequently, the cell was kept at 2.05 V and potentiostatically discharged until the current dropped to 10^{-5} A. To study the decomposition of Li_2S, the assembled fresh cell was first discharged to 1.7 V to completely convert sulfur to Li_2S. The cell was then charged to 2.4 V at constant current and held at 2.4 V until the current dropped to 10^{-5} A. Finally, the nucleation and decomposition capacity of Li_2S could be calculated by plotting the integral area of the curve through Faraday's Law.

Assembly of symmetric cells

0.2 mol L^{-1} Li_2S_6 was obtained by dosing Li_2S and S at a molar ratio of 1:5 into DME/DOL solution containing 1 mol L^{-1} LiTFSI and 2 wt% $LiNO_3$. 20 μL Li_2S_6 solution served as the electrolyte. The CV measurement was carried out with a voltage window from -1 to 1 V at a scan rate of 3 mV s^{-1}.

Theoretical calculations

All DFT calculations were carried out by the Vienna ab initio Simulation Package (VASP). The Perdew-Burke-Ernzerhof (PBE) exchange-correlation functional and projector augmented wave (PAW) pseudopotential were adopted with spin-polarization. During the structure optimization, the convergence criterion of total energy was set to 10^{-6} eV, and the atoms were relaxed until the force acting on each atom was less than 0.05 eV/Å. Gaussian smearing of 0.05 eV to the orbital occupation is applied. A plane-wave cut-off energy of 480 eV was used in all computations. The

Brillouin-zone integrations were conducted using Monkhorst-Pack (MP) grids of special points with the separation of 0.08 $Å^{-1}$. Each slab model was separated from its neighbors by 15 Å vacuum layer spacing. DFT-D3 method of Grimme with zero-damping function were used in van der Waals (vdW) corretions.

All adsorptive binding energies (Eads) used in this paper were defined as:

$$E_{ads} = E_{total} - (E_{slab} + E_{adsorbate})$$

where the E_{total} is the total energy of the slab/adsorbate interacting system and E_{slab} and $E_{adsorbate}$ are the energies of the slab and the isolated adsorbate, respectively.

S2 Figures and tables

S2.1 Figures:

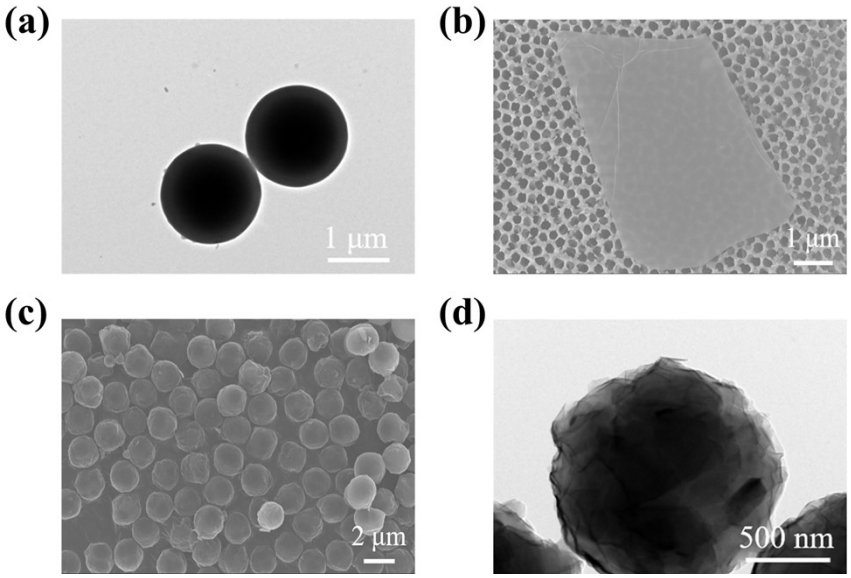

Figure S1 (a) TEM image of PMMA, (b) SEM image of single layer Ti_3C_2, (c) SEM image, and (d) TEM image of assembled MXene/PMMA precursors.

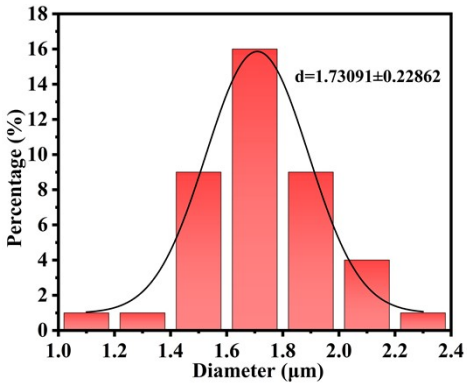

Figure S2 The particle size distribution of Ti_3C_2@N-CNTs.

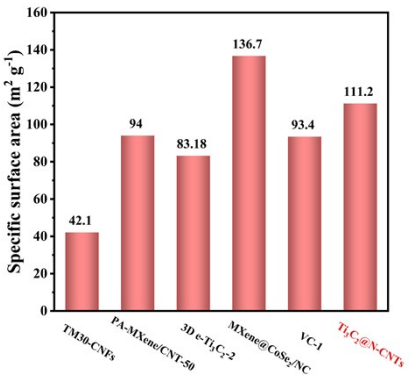

Figure S3 Comparison of Ti_3C_2@N-CNTs and recent work on improved specific surface area[1-5].

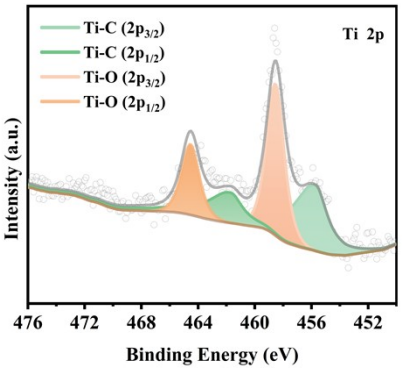

Figure S4 Ti 2p spectrum of Ti_3C_2@N-CNTs.

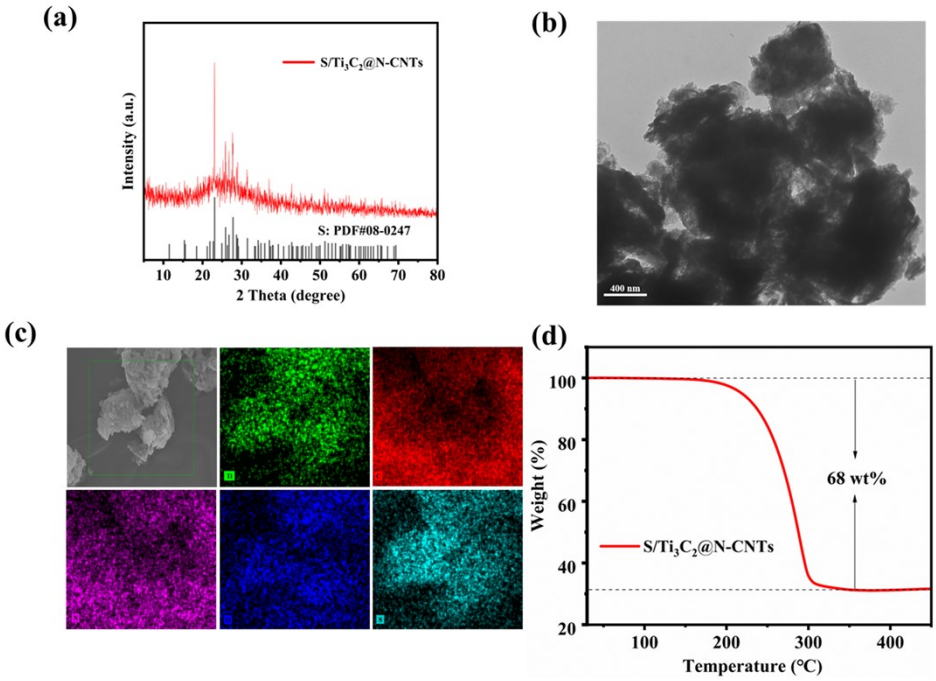

Figure S5 (a) XRD pattern, (b) TEM image, (c) elemental mappings, and (d) TGA curves of S/Ti_3C_2@N-CNTs.

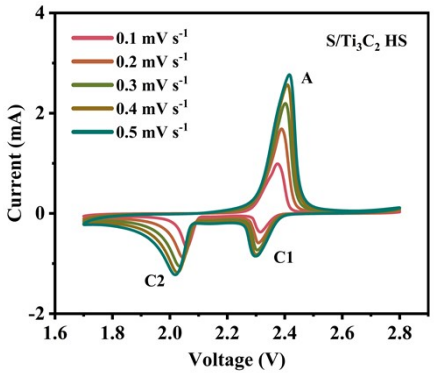

Figure S6 CV curves of the S/Ti_3C_2 HS electrode at scan rates of 0.1-0.5 mV s^{-1}.

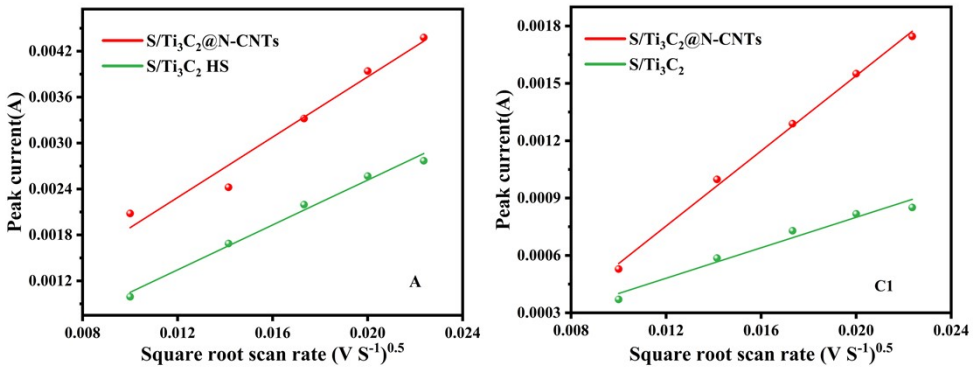

Figure S7 Linear fits the peak current values of the cells with S/Ti_3C_2@N-CNTs and S/Ti_3C_2 HS based on the CV curves.

The diffusion coefficient of cathodes can be calculated by the classical Randles-Sevcik equation :

$$I_P = 2.69 \times 10^5 \times n^{3/2} \times A \times D^{1/2} \times C_{Li} \times v^{1/2}$$

where I_p is the peak current (A), n is the charge transfer number (n = 2 for LSBs), A is the area of the cathode (~1.13 cm^2), D is the Li^+ diffusion coefficient ($cm^2 \cdot s^{-1}$), C_{Li} is the concentration of Li^+ in the material (1 $mol \cdot L^{-1}$), and ν is the scan rate ($V \cdot s^{-1}$). Because n, A, and C_{Li} are unchanged, a linear relationship between the peak current (I_{C1}, I_{C2}, I_A) and the square root of scanning rates ($I_p/v^{1/2}$) can represent the lithium-ion diffusion rate.

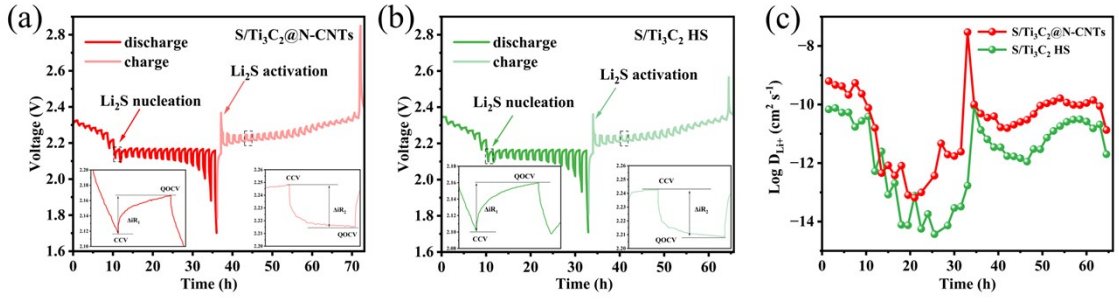

Figure S8 (a,b) Galvanostatic intermittent titration technique (GITT) curves of the different electrodes,(c) Migration coefficients of the Li^+.

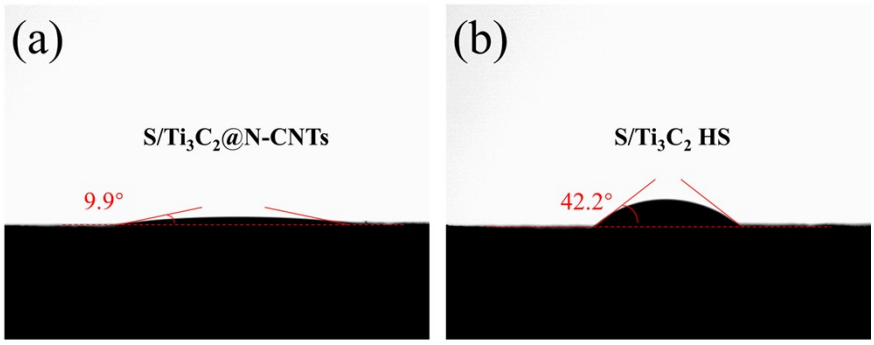

Figure S9 Contact angles of (a) S/Ti_3C_2@ N-CNTs, (b) S/Ti_3C_2 HS by using electrolytes.

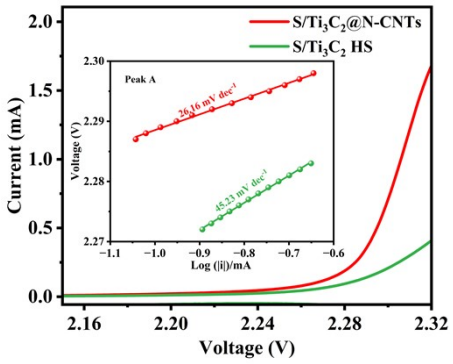

Figure S10 LSV curves of S/Ti_3C_2 HS and S/Ti_3C_2@ N-CNTs toward LiPSs oxidation, inset is the Tafel curve calculated from the peak A.

S2.2 Tables:

Table S1. Summary of element contents in Ti_3C_2@N-CNTs determined by XPS.

Sample (at%)	Ti	C	N	O
Ti_3C_2@N-CNTs	14.44	58.31	7.5	19.75

Table S2. Nitrogen species of N 1s in Ti_3C_2@N-CNTs determined by XPS.

Content (%)	Pyridinic-N	Pyrrolic-N	Graphitic-N
Ti_3C_2@N-CNTs	57.01	11.72	31.27

Table S3 Summary of recent reports on sulfur host cathodes for LSBs compared with Ti_3C_2@N-CNTs.

Host material	Sulfur loading (mg cm^{-2})	Current density (C)	Cycle number	Initial capacity (mAh g^{-1})	Decay rate (per cycle, %)	Reference
Ti_3C_2@N-CNTs	1.2-1.4	0.2	200	1214	0.048	This work
		1	1000	821	0.015	
$Ti_3C_2T_x$-CNTs	1.6	0.2	100	1368	0.233	6
		1	500	902	0.062	
TiS_2/TiO_2@MXene	1.5	0.1	100	1232	0.133	7
NLi_2S@LPS/TNS	1.5-2.0	0.2	100	-	0.08	8
MXene@$CoSe_2$/NC	1.7	0.2	400	1063.14	0.06	9
S-MXeneSH(CH)	-	1	500	880	0.0375	10
NG/WSe_2	1	1	500	923	0.037	11
$ZnCo_2O_4$@Ti_3C_2	1.0-1.5	0.5	400	1142	0.183	12
Co_9S_8@MoS_2	3	1	400	794	0.091	13
Ti_3C_2/C	1	1	500	822	0.05	14
TM-CNFs	1.5-2	0.5	200	870.2	0.036	15
		1	500	~900.5	0.039	
$MoSe_2$@C/rGO/S	1.2-1.5	1	300	851	0.1	16

References：

1. B. Zhang, C. Luo, G. Zhou, Z. Pan, J. Ma, H. Nishihara, Y. He, F. Kang, W. Lv and Q. Yang, *Adv Funct Materials*, 2021, **31**, 2100793.
2. T. Wang, D. Luo, Y. Zhang, Z. Zhang, J. Wang, G. Cui, X. Wang, A. Yu and Z. Chen, *ACS Nano*, 2021, **15**, 19457-19467.
3. T. Li, L. Liang, Z. Chen, J. Zhu and P. Shen, *Chemical Engineering Journal*, 2023, **474**, 145970.
4. L. Chen, Y. Sun, X. Wei, L. Song, G. Tao, X. Cao, D. Wang, G. Zhou and Y. Song, *Advanced Materials*, 2023, **35**, 2300771.
5. Y. Li, J. Chen, P. Cai and Z. Wen, *J. Mater. Chem. A*, 2018, **6**, 4948-c4954.
6. M. Xu, L. Liang, J. Qi, T. Wu, D. Zhou and Z. Xiao, *Small*, 2021, **17**, 2007446.
7. V. P. Nguyen, J. S. Park, H. C. Shim, J. M. Yuk, J. Kim, D. Kim and S. Lee, *Adv Funct Materials*, 2023, **33**, 2303503.
8. C. Cui, R. Meng, S. Song, P. Paoprasert, L. Zhang, X. He and X. Liang, *Journal of Power Sources*, 2023, **571**, 233050.
9. T. Li, L. Liang, Z. Chen, J. Zhu and P. Shen, *Chemical Engineering Journal*, 2023, **474**, 145970.
10. X. Geng, C. Liu, C. Zhao, Z. Jiang, E. G. Lim, Y. Wang, I. Mitrovic, L. Yang and P. Song, *Electrochimica Acta*, 2023, **441**, 141877.
11. C. Zhang, B. Fei, D. Yang, H. Zhan, J. Wang, J. Diao, J. Li, G. Henkelman, D. Cai, J. J. Biendicho, J. R. Morante and A. Cabot, *Adv Funct Materials*, 2022, **32**, 2201322.
12. A. Wei, L. Wang and Z. Li, *Journal of Alloys and Compounds*, 2022, **899**, 163369.
13. Q. Hao, G. Cui, Y. Zhang, J. Li and Z. Zhang, *Chemical Engineering Journal*, 2020, **381**, 122672.
14. H.-Y. Zhou, Z.-Y. Sui, K. Amin, L.-W. Lin, H.-Y. Wang and B.-H. Han, *ACS Appl. Mater. Interfaces*, 2020, **12**, 13904-13913.
15. R. Hou, S. Zhang, P. Zhang, Y. Zhang, X. Zhang, N. Li, Z. Shi and G. Shao, *J. Mater. Chem. A*, 2020, **8**, 25255-25267.
16. C. Li, W. Ge, S. Qi, L. Zhu, R. Huang, M. Zhao, Y. Qian and L. Xu, *Advanced*

Energy Materials, 2022, **12**, 2103915.